

## Vibrational effects on the electron momentum distributions of valence orbitals of formamide

Y. R. Miao, J. K. Deng, and C. G. Ning

Citation: *J. Chem. Phys.* **136**, 124302 (2012); doi: 10.1063/1.3696028

View online: <http://dx.doi.org/10.1063/1.3696028>

View Table of Contents: <http://jcp.aip.org/resource/1/JCPSA6/v136/i12>

Published by the [American Institute of Physics](#).

---

### Additional information on *J. Chem. Phys.*

Journal Homepage: <http://jcp.aip.org/>

Journal Information: [http://jcp.aip.org/about/about\\_the\\_journal](http://jcp.aip.org/about/about_the_journal)

Top downloads: [http://jcp.aip.org/features/most\\_downloaded](http://jcp.aip.org/features/most_downloaded)

Information for Authors: <http://jcp.aip.org/authors>

#### ADVERTISEMENT

**AIP**Advances

*Submit Now*

### Explore AIP's new open-access journal

- Article-level metrics now available
- Join the conversation! Rate & comment on articles

# Vibrational effects on the electron momentum distributions of valence orbitals of formamide

Y. R. Miao, J. K. Deng, and C. G. Ning<sup>a)</sup>

*Department of Physics, State Key Laboratory of Low-Dimensional Quantum Physics, Tsinghua University, Beijing 100084, People's Republic of China*

(Received 21 December 2011; accepted 5 March 2012; published online 22 March 2012)

The ionization energy spectra and electron momentum distributions of formamide were investigated using the high-resolution electron momentum spectrometer in combination with high level calculations. The observed ionization energy spectra and electron momentum distributions were interpreted using symmetry adapted cluster-configuration interaction theory, outer valence Green function, and DFT-B3LYP methods. The ordering of  $10a'$  and  $2a''$  orbitals of formamide was assigned unambiguously by comparing the experimental electron momentum distributions with the corresponding theoretical results, i.e.,  $10a'$  has a lower binding energy. In addition, it was found that the low-frequency wagging vibration of the amino group at room temperature has noticeable effects on the electron momentum distributions. The equilibrium-nuclear-positions-approximation, which was widely used in electron momentum spectroscopy, is not accurate for formamide molecule. The calculations based on the thermal average can evidently improve the agreement with the experimental momentum distributions. © 2012 American Institute of Physics. [<http://dx.doi.org/10.1063/1.3696028>]

## I. INTRODUCTION

Formamide ( $\text{HCONH}_2$ ), containing a C–N–O linkage, is the simplest model of the peptide bond. The electronic structure of formamide is not only important for spectroscopy but also for biology and chemistry. The elucidation of the electronic state of formamide is essential for us to understand the spectroscopy of protein. Interestingly, formamide can be formed on synthetic interstellar and cometary ices after UV photolysis at 20 K and subsequent warming to 200 K.<sup>1</sup>

The geometric structure of formamide has been of interest to chemists for a long time. The planarity of formamide is an extremely controversial topic which lasts for nearly 60 years until now.<sup>2–9</sup> Although controversial viewpoints exist, non-planarity effect is very small.<sup>8,9</sup> Therefore, the planar structure was taken as the equilibrium structure for the calculations in present work.

The electronic structures of formamide has been investigated experimentally and theoretically using photoelectron spectroscopy (He I,<sup>10</sup> He II,<sup>11</sup> and x-ray (Refs. 12 and 13)) and configuration interaction (CI) theoretical method.<sup>13</sup> Recently, Brion *et al.* reported the momentum distribution of the first peak of formamide.<sup>14</sup> They observed a significant discrepancy between the measured momentum distributions of the  $10a'+2a''$  orbitals and the plane-wave-impulse-approximation (PWIA) calculations.<sup>15</sup> The discrepancy particularly occurred in the low momentum region ( $<1$  a.u.), which was tentatively attributed to the distorted wave effects.<sup>16–18</sup> According to our best knowledge, there is no detailed electron momentum spectroscopy (EMS) experimental result for the whole valence region of formamide reported previously.

The equilibrium-nuclear-positions-approximation (ENPA) is widely used in most EMS studies,<sup>15</sup> which assumes that the vibrational effects on the momentum distributions are negligible. However, several recent works have found that the large amplitude vibration modes of some floppy molecules can evidently change the momentum distributions.<sup>19–24</sup> Formamide has a low frequency anharmonic vibrational mode ( $287\text{ cm}^{-1}$ ),<sup>25,26</sup> which is related to the large amplitude wagging motion of  $\text{NH}_2$  group.<sup>25,26</sup> Present work showed that the vibration has notable effects on the momentum distributions of valence orbitals of formamide, and the thermally averaged calculations can describe the observed momentum distributions better than the ENPA calculation.

The experiment was conducted on our high-resolution electron momentum spectrometer at various impact energies (600 eV and 1500 eV). The distorted wave effects suggested by Brion *et al.*<sup>14</sup> were confirmed in present work. Moreover, the discrepancy they observed is also partly due to the vibrational effects.

Another motivation of the present work is that formamide has congested satellite lines, which result from the electron correlation during the ionization in the inner-valence region and outer-valence region.<sup>13</sup> Therefore, formamide can also serve as a good prototype for studying electron correlations. Recently, we have introduced the high level symmetry adapted cluster-configuration interaction (SAC-CI) theoretical method for directly calculating the momentum distributions of Dyson orbitals.<sup>27,28</sup> In the present work, the powerful SAC-CI method was employed to interpret the experimental results of both binding energy spectra (BES) and momentum distributions. Moreover, Hartree-Fock (HF),<sup>29</sup> density functional theory (DFT),<sup>30,31</sup> and outer valence Green function (OVGF; Refs. 32 and 33) calculations were also presented.

<sup>a)</sup>Electronic mail: ningcg@tsinghua.edu.cn.

## II. EXPERIMENTAL AND THEORETICAL METHODS

Electron momentum spectroscopy is based on (e, 2e) reaction, where one electron comes in and two electrons go out.<sup>15,34,35</sup> The non-coplanar symmetric geometry is used in our spectrometer. Detailed descriptions of the spectrometer have been reported previously.<sup>36,37</sup> Using high energy ( $\sim 1$  keV for atoms and molecules) incident electron beam, electronic structures, especially the ionization energy and the momentum distribution of individual Dyson orbital<sup>38–41</sup> of the sample molecule can be extracted when the single ionizing collision takes place at Bethe ridge.<sup>15</sup> The kinematics of the incoming and two outgoing electrons can be completely determined through the coincidental measurement. The magnitude of the momentum ( $p$ ) of the electron before struck out is given by<sup>15</sup>

$$p = \left[ (2p_1 \cos \theta_1 - p_0)^2 + \left[ 2p_1 \sin \theta_1 \sin \left( \frac{\phi}{2} \right) \right]^2 \right]^{1/2}, \quad (1)$$

where  $p_0$  and  $p_1$ , respectively, represent the momentum of the incident electron and the outgoing electron,  $\theta$  is the polar angle of the outgoing electron relative to the incident electron beam ( $\theta_1 = \theta_2 = 45^\circ$ ), and  $\phi$  is the relative azimuthal angle between the two outgoing electrons. Under the condition of the high momentum transfer and the high incident energy, the differential cross-section of EMS with PWIA can be given by<sup>15</sup>

$$\sigma_{\text{EMS}} = \frac{d^5 \sigma}{d\Omega_1 d\Omega_2 dE_1} \propto \frac{1}{4\pi} S_i^s \int d\Omega | \langle e^{-i\mathbf{p}\cdot\mathbf{r}} \psi_i^{N-1} | \psi_g^N \rangle |^2. \quad (2)$$

The differential cross section is proportional to the spectroscopic factor  $S_i^s$ . The ground state and the ionized state of the target are represented by  $\psi_g^N$  and  $\psi_i^{N-1}$ , respectively.  $N$  is the total electron number. The term  $\langle e^{-i\mathbf{p}\cdot\mathbf{r}} \psi_i^{N-1} | \psi_g^N \rangle$  is called Dyson orbital in momentum space.<sup>15,42</sup> Here,  $\int d\Omega$  represents the spherical average for the randomly oriented molecules in gas phase. Dyson orbitals can be approximated using Hartree-Fock orbitals or Kohn-Sham orbitals for simplifying the calculation.<sup>15,28,30</sup>

In the present experiment, the instrumental energy resolution is 0.68 eV (full width at half maximum), which was obtained through the calibration of Ar sample. The finite spectrometer acceptance angle of  $\theta$  is  $\pm 0.84^\circ$  (one standard error), and the angle resolution of azimuthal angle  $\varphi$  is  $\pm 0.53^\circ$  (one standard error). A commercial sample formamide with a purity of 99.9% was used directly without further purifications. No impurities were evidently observed in the binding energy spectrum.

The SAC-CI (Refs. 43–45) method is a cluster expansion formalism for the study of electron correlations in ground state and various kinds of excited states. The SAC-CI method has been developed by the Nakatsuji laboratory both in theories and algorithms.<sup>46–49</sup> SAC-CI theory has shown being a reliable and powerful tool for investigating a wide variety of chemistry, molecular spectroscopy, and electron momentum spectroscopy.<sup>26,27,50–56</sup> There are two options in SAC-CI calculations: SAC-CI single and double R excitation operator (SD-R) method is useful for the single excitation,

and SAC-CI general-R method is reliable for the multiple excitation process. The latter method was used in present work. The SAC-CI combined the merits of size consistency of the cluster expansion<sup>57,58</sup> and the energy upper boundary of CI.<sup>59</sup>

Present SAC-CI calculations for formamide were performed with the GAUSSIAN 03 suite of programs.<sup>60</sup> The calculation employed the correlation consistent basis set aug-cc-pVTZ.<sup>61</sup> The active space included 60 molecular orbitals. Higher-order linked operators were generated by exponential generation algorithm.<sup>45–47</sup> R operators up to quadruples were included. Perturbation selections were done to reduce the computational time. The threshold of the linked terms for the ground state was set to  $\lambda_g = 1.0 \times 10^{-6}$ . The unlinked terms were included as the products of the linked terms whose single and double configuration interaction (SDCI) coefficients were larger than  $5.0 \times 10^{-3}$ .<sup>46,49</sup>

## III. RESULTS AND DISCUSSION

### A. Binding energy spectra of formamide

Formamide has  $C_s$  symmetry at ground neutral  $1A'$  state. Its electronic configuration can be written as

$$\underbrace{(1a')^2(2a')^2(3a')^2}_{\text{core}} \underbrace{(4a')^2(5a')^2}_{\text{inner valence}} \times \underbrace{(6a')^2(7a')^2(8a')^2(9a')^2(1a'')^2(2a'')^2(10a')^2}_{\text{outer valence}}.$$

The BES of formamide measured at the impact energy of 1500 eV plus binding energies was shown in Fig. 1(a). There are eight resolved ionization peaks as labeled 1–8. To obtain individual electron momentum distribution, 11 Gaussian peaks are employed to fit the measured BES at each azimuthal angle. The ionization potentials of outer-valence orbitals were obtained from the x-ray photoelectron spectrum (XPS; Ref. 13) and He II photoelectron spectrum.<sup>11</sup> The widths of the Gaussian peaks were combinations of the present experimental energy resolution and Frank-Condon widths of the corresponding ionization bands determined by the He II PES. Small adjustments have been made to compensate the asymmetry of the Frank-Condon profiles. In the outer-valence region, present work agrees well with the previous XPS results. Detailed results were listed in Table I. Additional structures in the binding energy spectrum of formamide in the inner-valence region (22–35 eV) were also observed in the present (e, 2e) study in Fig. 1(a). As shown in Fig. 1(b), the SAC-CI general-R method can well describe the measured binding energy spectra in the whole valence region.

The SAC-CI calculation predicted seven main lines at 9.60, 9.93, 13.60, 14.19, 16.08, 18.23, and 20.56 eV corresponding to the  $(10a')$ ,  $(2a'')$ ,  $(1a')$ ,  $(9a')$ ,  $(8a')$ ,  $(7a')$ , and  $(6a')$  one-hole states. In inner-valence region, many congested satellite lines appeared, which were attributed to the many-body effects. As compared in Table I, only the SAC-CI method, which considered multiple excitations, can produce a detailed description of the satellite peaks below peak 4 and peak 5. In Fig. 1(a), peak 6, 7, and 8 showed broad bands due to the severe excitation-ionization process.

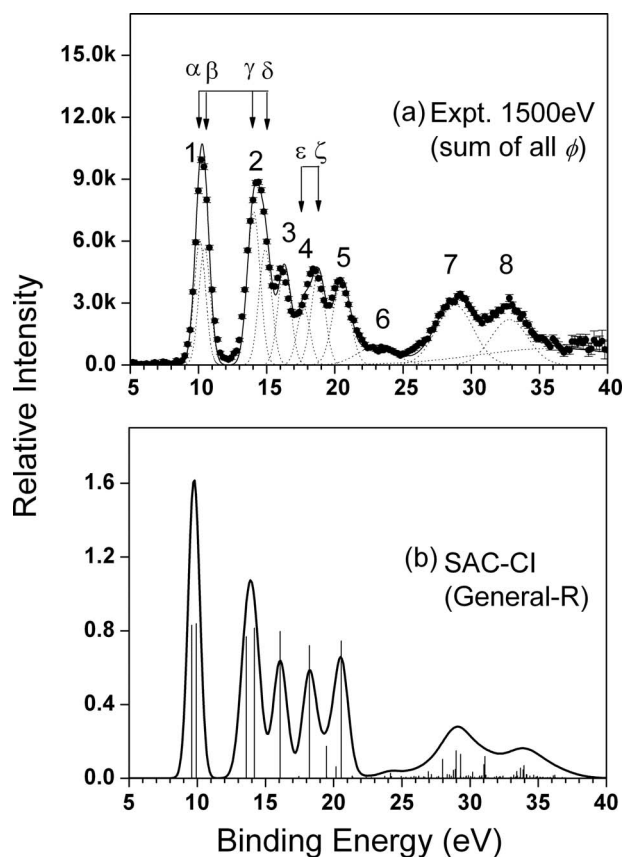


FIG. 1. Binding energy spectra of formamide. (a) The experimental ( $2e$ ) ionization spectrum summed over all  $\phi$  angles at impact energy of 1500 eV plus binding energies. Peaks were designated using the symmetry labels of planar geometry. (b) Theoretical simulation of the binding energy spectrum using SAC-CI general-R method. The heights of vertical spikes represent the calculated spectroscopic factors.

In present work, we also calculated the vertical ionization energies of formamide using DFT-B3LYP (Becke-3-parameter-Lee-Yang-Parr).<sup>62,63</sup> In Table I,  $\Delta B3LYP$ , as mentioned in Ref. 9, stands for the total energy difference between the valence-hole cation and the neutral ground state of the molecule. In Table I, we found that  $\Delta B3LYP$  method provided an excellent prediction of the vertical ionization energies of formamide. OVGf theory also presented very accurate ionization potentials in outer-valence region as shown in Table I.

## B. Thermal average of momentum distributions of valence orbitals

The momentum profiles of molecular orbitals are dependent on the molecular geometric structure. Therefore, the statistical averaged momentum distribution may be different from the momentum distribution of equilibrium structure. For example, the low frequency vibrational modes notably change the momentum distributions of the highest occupied molecular orbital of  $W(CO)_6$ .<sup>64</sup>

Formamide easily deviates from its equilibrium configuration due to the very shallow and wide potential valley, which is related to the wagging vibration mode of amino group, as

illustrated in Fig. 2. The vibrational frequency of the wagging mode was measured as  $287\text{ cm}^{-1}$  by King.<sup>26</sup>

The wagging motion can be well approximated by one-dimensional anharmonic oscillator model, as shown in Fig. 3(b). The populations (in parentheses) at each energy level were calculated using Boltzmann distributions. At room temperature (300 K), formamide mainly stays at the vibrational ground state (77.3%), and has 19.0% population at the first vibrational excited state.

The valence orbitals energies of formamide at different amino-wagging angles are illustrated in Fig. 4. It should be noted that the orbital ordering did not change during the large amplitude wagging motion and the valence orbital energies of formamide are not sensitive to the wagging vibration.

To calculate the thermal averaged momentum distributions, it was assumed that the electron could immediately follow the nuclear motions. If neglecting the population at the vibrational level  $j \geq 4$ , the thermal averaged momentum distribution  $\rho_{av}(p)$  can be given by

$$\rho_{av}(p) = \sum_n \rho_{\tau_n}(p) \frac{\sum_{j=0}^3 e^{-\frac{E_j}{kT}} \int_{\tau_n - \frac{\epsilon}{2}}^{\tau_n + \frac{\epsilon}{2}} |\Phi_j(\tau)|^2 d\tau}{\sum_{j=0}^3 e^{-\frac{E_j}{kT}}}, \quad (3)$$

where  $\rho_{\tau_n}(p)$  is the momentum distributions when formamide with a wagging angle  $\tau_n$ ,  $\Phi_j(\tau)$  is  $j$ th vibrational wavefunction for the wagging mode,  $E_j$  is  $j$ th vibrational energy level,  $\tau$  is the wagging angle,  $T$  is the temperature, and  $\epsilon$  was the angle step for calculating the integral in (3) ( $\epsilon = 5^\circ$  in the present calculation). The relative population versus the wagging angle  $\tau$  was plotted in Fig. 3(a). It can be seen that the most probable conformation of formamide at room temperature is planar. However, the possibility of formamide staying near the planar geometry is not high, only about 29% within  $[-10^\circ, 10^\circ]$  of the wagging angle range.

The thermally and spherically averaged momentum distributions of valence orbitals were shown in Fig. 5 in comparison with the momentum distribution at the equilibrium geometry. The calculation used B3LYP exchange-correlation functional and the correlation consistent basis set aug-cc-pVTZ.<sup>61</sup> The vibrationally averaged distributions were shown with the red line designated by 2, while the equilibrium geometry momentum distributions with a black line designated by 1. From Figs. 5(a)–5(c), 5(e), 5(f), 5(h), and 5(i), we can conclude that the effects of averaging over anharmonic wagging vibration are observable and can evidently change the momentum distributions. However, the vibration has little effect on the momentum distributions of molecular orbitals  $9a'$  and  $6a'$  as shown in Figs. 5(d) and 5(g), which may be due to the different electron density distributions around the amino group in these two orbitals.

## C. Momentum distributions of peak 1 and peak 2

Electron momentum distributions for the first four valence orbitals were displayed in Fig. 7. The ordering of the first two orbitals has ever been debated.<sup>65–67</sup> At the level of

TABLE I. Ionization potentials (eV) and spectroscopic factors (in parentheses) of formamide.

EMS <sup>a</sup>		PES <sup>b</sup>	PES <sup>c</sup>	SAC-CI <sup>a</sup>	CI <sup>c</sup>	OVGf <sup>a</sup>	$\Delta$ B3LYP <sup>a</sup>
Peak 1	10.10 (0.83) <sup>d</sup>	10.4	10.42	9.60 (0.83)	10.72 (0.89)	10.496 (0.91)	10.29 (10a')
	10.45 (0.84) <sup>d</sup>	10.7	10.87	9.93 (0.84) <sup>e</sup>	10.92 (0.92)	10.726 (0.90)	10.70 (2a'')
Peak 2	14.05 (0.77) <sup>d</sup>	14.1	14.17	13.60 (0.77) <sup>e</sup>	14.42 (0.82)	14.464 (0.88)	14.36 (1a'')
	14.90 (0.82) <sup>d</sup>	14.8	14.89	14.19 (0.82)	15.43 (0.88)	15.181 (0.91)	14.61 (9a')
Peak 3	16.30 (0.80) <sup>d</sup>	16.3	16.48	16.08 (0.80)	17.26 (0.84)	16.939 (0.90)	16.48 (8a')
Peak 4	17.70 (0.37)	17.8	17.41	18.23 (0.72)	19.60 (0.69)		
	18.77 (0.61)	18.8	18.79	19.47 (0.17)	20.71 (0.22)	19.056 (0.90)	18.70 (7a')
Peak 5	20.48 (0.81)	20.7	20.47	20.17 (0.06) <sup>e</sup>	22.55 (0.59)		20.48 (6a')
			21.67	20.56 (0.75)			
Peak 6	23.0 (0.20)		23.77	21.36 (0.01)	23.20 (0.07)		
				23.75 (0.01)	25.21 (0.03)		
				24.16 (0.03)			
				24.24 (0.01)			
				26.94 (0.04)			
Peak 7	28.8 (0.59)	28.5	28.4	27.16 (0.02)			28.37 (5a')
				28.00 (0.10)			
				28.32 (0.02)			
				28.49 (0.02)			
				28.63 (0.01)			
				28.79 (0.04)			
				28.92 (0.05)			
				28.98 (0.15)			
				29.29 (0.01)			
				29.31 (0.13)			
Peak 8	32.8 (0.32)		33	33.20 (0.02)	31.04 (0.14)		32.07 (4a')
				33.43 (0.04)	33.43 (0.10)		
				33.48 (0.01)			
				33.70 (0.06)			
				33.90 (0.05)			
				33.97 (0.07)			
				34.12 (0.02)			
				34.16 (0.02)			
				34.39 (0.01)			
			34.68 (0.02)				

<sup>a</sup>Present work. OVGf and SAC-CI calculations were executed in GAUSSIAN 03 program suite,<sup>60</sup> and  $\Delta$ B3LYP was done in ADF program.<sup>70</sup>

<sup>b</sup>From Ref. 11.

<sup>c</sup>From Ref. 13.

<sup>d</sup>The spectroscopic factor given by SAC-CI was directly used for normalizing the experimental momentum distributions.

<sup>e</sup>Dyson orbitals belong to A'' state, while others belong to A' state.

HF/aug-cc-pVTZ, the 2a'' orbital was calculated to have the lowest ionization potential while B3LYP with the same basis set tends to place the 10a' at a lower energy. EMS can provide a unique way for unambiguous orbital assignment<sup>68</sup> by simply comparing the experimental momentum profiles with the theoretical calculations as illustrated in Figs. 7(a) and 7(b). The momentum distributions of the first two orbitals can be roughly reproduced by B3LYP/aug-cc-pVTZ calculations, and obviously the orbital ordering given by HF method mismatched the two distributions. Therefore, we unambiguously assigned 10a' to peak  $\alpha$ , and 2a'' to peak  $\beta$ . Note that the calculations overestimate the measured intensity of peak  $\alpha$  in the region 0.5 to 1.5 a.u. while underestimate that of peak  $\beta$  in the region 0 to 1.5 a.u. The discrepancy might be due to that peak  $\alpha$  and peak  $\beta$  are too close. The ionization potential difference is only 0.4 eV, which cannot be well resolved by our current experimental energy resolution. Therefore, their summed intensity was compared with the calculations in Fig. 7(c). DFT-B3LYP calculations using equilibrium

configuration (line 1) produced a better description of the experimental momentum profiles than HF method (line 3), especially in the low momentum region 0 to 0.5 a.u. The thermal averaged DFT-B3LYP calculation (line 2) further improved the agreement with the experimental results.

It is worth noting that the distorted wave effect was also observed in the low momentum region for peak  $\beta$  in Fig. 7(b). The observed momentum distributions depend on the impact energy. At higher impact energy (1500 eV), the discrepancy with PWIA calculations becomes less. Interestingly, the 2a'' orbital exhibits d-like characteristics (see Fig. 6(b)). The similar phenomena were also observed in several d-like orbitals of other molecules.<sup>16–18,69</sup>

The experimental momentum distributions of peaks  $\gamma$  and  $\delta$  were compared with DFT calculations in Figs. 7(d) and 7(e), respectively. The calculations underestimate the measured intensity of peak  $\gamma$  in the region 0 to 0.6 a.u., but they overestimate that of peak  $\delta$ . The discrepancies between the calculations and the measurements in Figs. 7(d) and 7(e) are

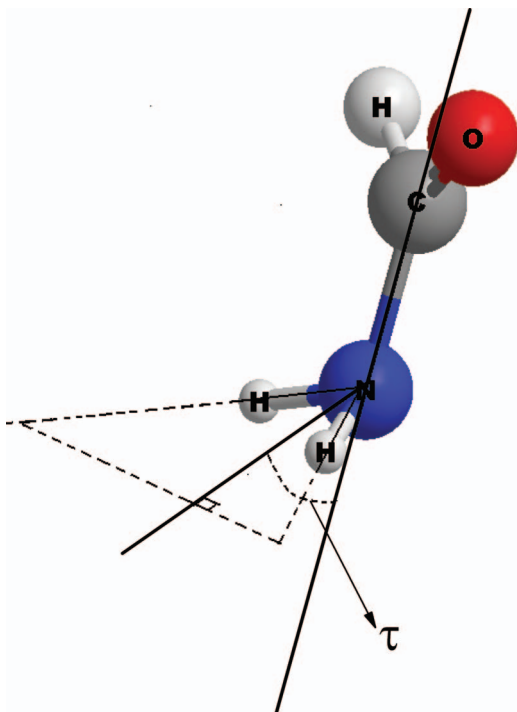
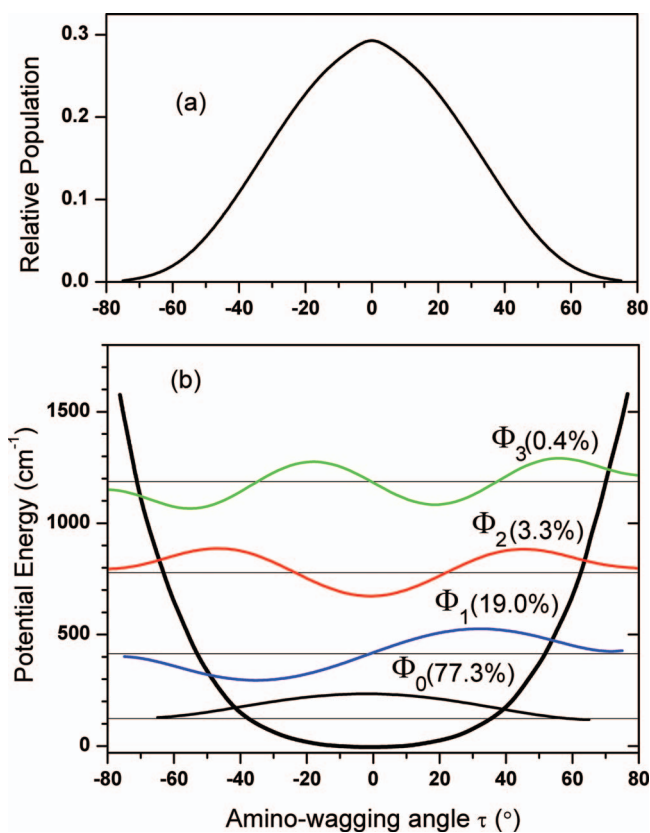
FIG. 2. Schematic of amino-wagging angle ( $\tau$ ).

FIG. 3. (a) Population of formamide at different amino-wagging angles ( $\tau$ ) at room temperature. (b) Potential energy curve (black thick line) and the first four vibrational wavefunctions of the wagging vibrational mode ( $\nu = 287 \text{ cm}^{-1}$ ; Ref. 26) were taken from Ref. 25. The number in parentheses represents the population of each energy level at room temperature.

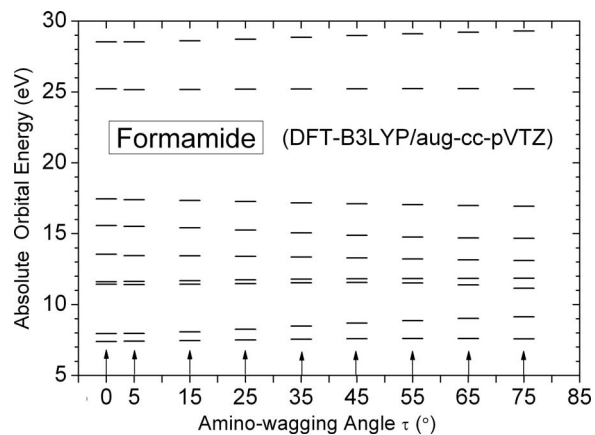


FIG. 4. Valence orbital energies of formamide at different amino-wagging angles.

largely due to the deconvolution procedure considering that two peaks are significantly overlapped. As shown in Fig. 7(f), their summed intensity distribution matched better with the corresponding calculations. The thermal averaged DFT calculation (line 2) produced a little better description than the equilibrium calculation (line 1) although not pronounced.

#### D. Momentum distributions of other orbitals

The momentum distributions of peak 3 were compared with the calculated distributions in Fig. 8(a). There are notable discrepancy between the experimental results and the thermal averaged calculation, which may be due to the overlap with the neighboring peaks.

In the previous XPS study of formamide, Lisini *et al.*<sup>13</sup> suggested that the ionization from  $7a'$  orbital leads to two structures in the spectrum with almost equal intensity. Two peaks  $\epsilon$  and  $\zeta$  were used for fitting data in Fig. 1(a) to extract

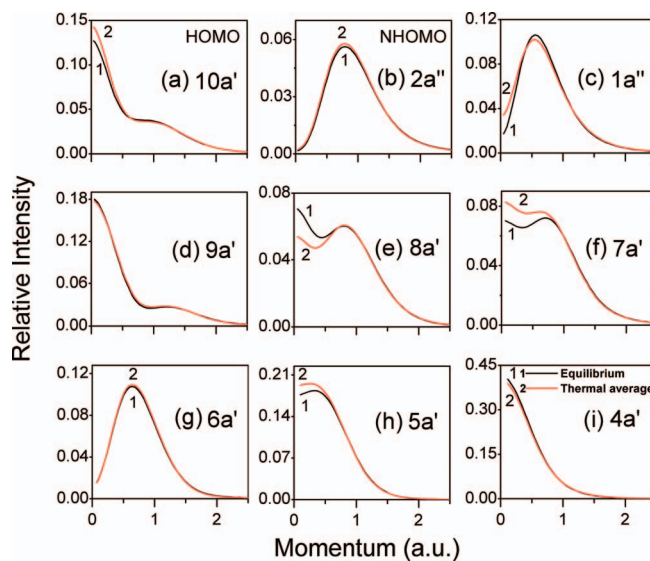


FIG. 5. Theoretical momentum distributions at equilibrium geometry and the thermal averaged momentum distributions for valence orbitals of formamide. The experimental momentum resolution has been folded. The corresponding electron density contours of these orbitals were plotted in Fig. 6.

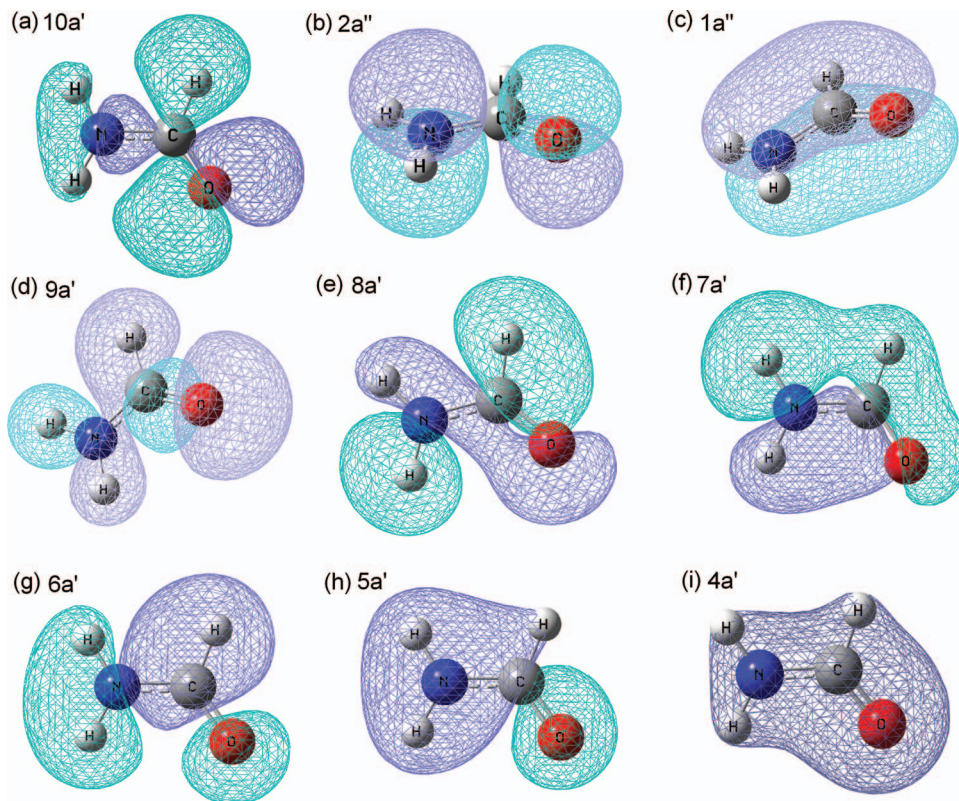


FIG. 6. Valence orbitals of formamide at the equilibrium geometry (contour value: 0.05).

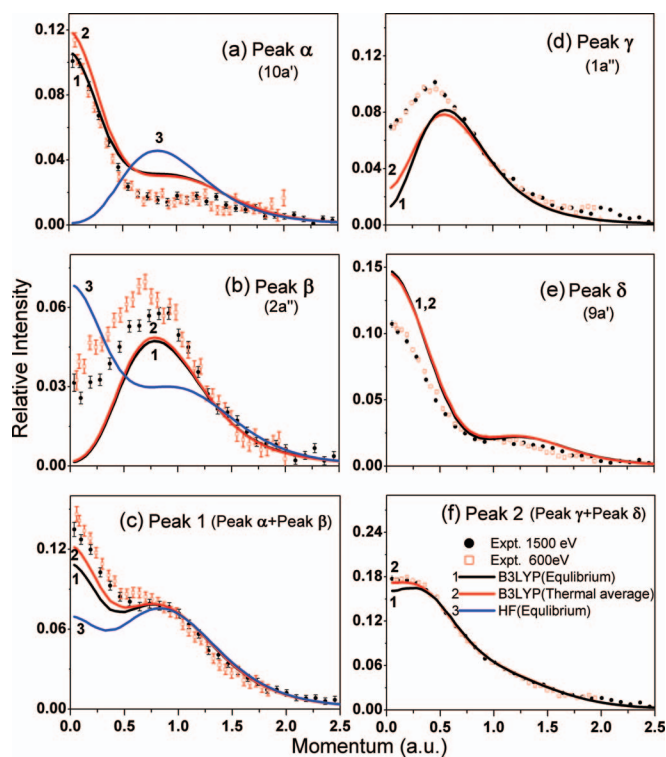


FIG. 7. Comparison of the experimental momentum distributions for peak  $\alpha$ ,  $\beta$ ,  $\gamma$ , and  $\delta$  with the theoretical calculations at equilibrium geometry and that with the thermal average. Curve 3 was plotted to illustrate the incorrect orbital assignment by HF method.

their momentum distributions. As shown in Figs. 8(b) and 8(c), experimental momentum distributions of the two structures were nearly the same, and can be described using the momentum distribution of  $7a'$  orbital. So, it can be concluded that these two peaks came from  $7a'$  orbital; the spectroscopic factor of peak  $\epsilon$  is 0.35, and 0.61 for peak  $\zeta$ . The obtained spectroscopic factors are different from present SAC-CI calculations and the previous results.<sup>13</sup> Further high energy resolution (e, 2e) experiments and high level calculations may help clarify this issue. The summed momentum distribution was compared with the corresponding theoretical calculations in Fig. 8(d). The thermal averaged calculation described the measured momentum distributions a little better in the low momentum region 0 to 1 a.u. than the equilibrium calculation.

The experimental momentum distributions of peak 5 were shown in Fig. 9(a) in comparison with the calculated results. The spectroscopic factors obtained through SAC-CI have been multiplied by the momentum distributions of their parent orbitals, which have taken account of vibrational effects using B3LYP/aug-cc-pVTZ method. The calculations are in excellent agreement with the experimental results. Since the orbital picture broke severely for peak 6, 7, and 8, the Dyson orbitals calculated using SAC-CI method at equilibrium were used directly for comparing with the experimental results in Figs. 9(b) and 9(d). The vibrational effects have not been considered because the computational cost is very high for the thermally averaged SAC-CI calculations. As it can be seen, the calculation successfully reproduced the

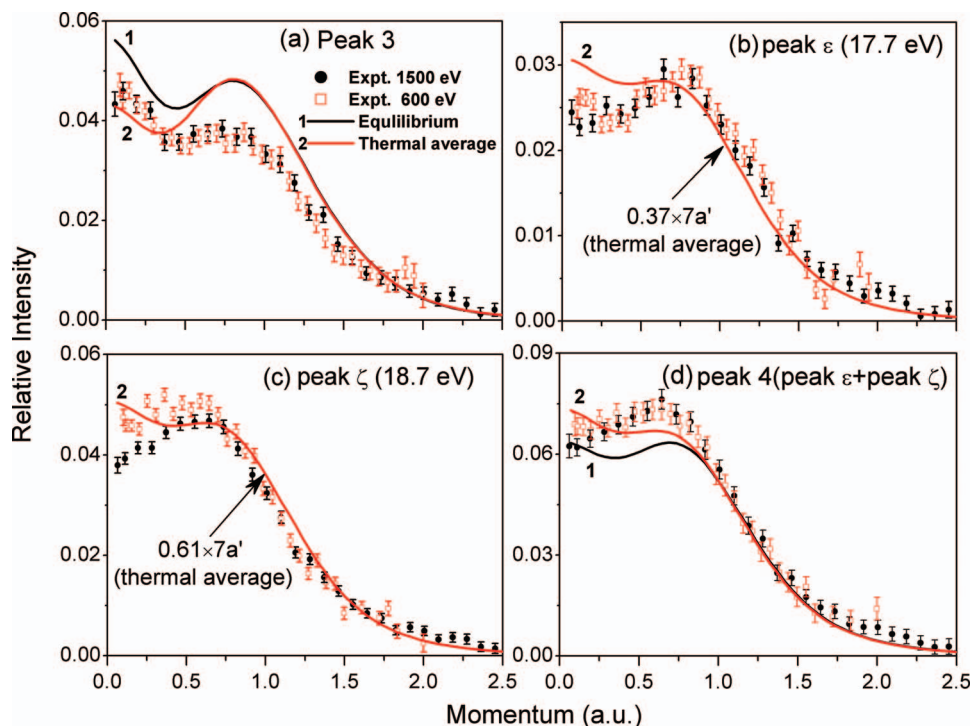


FIG. 8. Experimental and calculated momentum distributions of peak 3 and peak 4.

observed momentum distributions. In Table I, the spectroscopic factor of peak 6 was underestimated by SAC-CI method. The measured spectroscopic factor is 0.2 while SAC-CI predicted 0.06 (summed intensity), nevertheless the momentum profile was roughly reproduced by the calculation as shown in Fig. 9(b).

There are many congested satellite lines in the inner valence region 25 eV to 35 eV as shown in Fig. 1(a). The

vibrational effect is not significant in this region, and the momentum distributions calculated using SAC-CI method at the equilibrium geometry were compared with the measured momentum profiles. Peak 7 in Fig. 9(c) and peak 8 in Fig. 9(d) both exhibited s-type distributions, and the SAC-CI method can well reproduce the experimental momentum profiles. The main sources of these two peaks are shown in Table I.

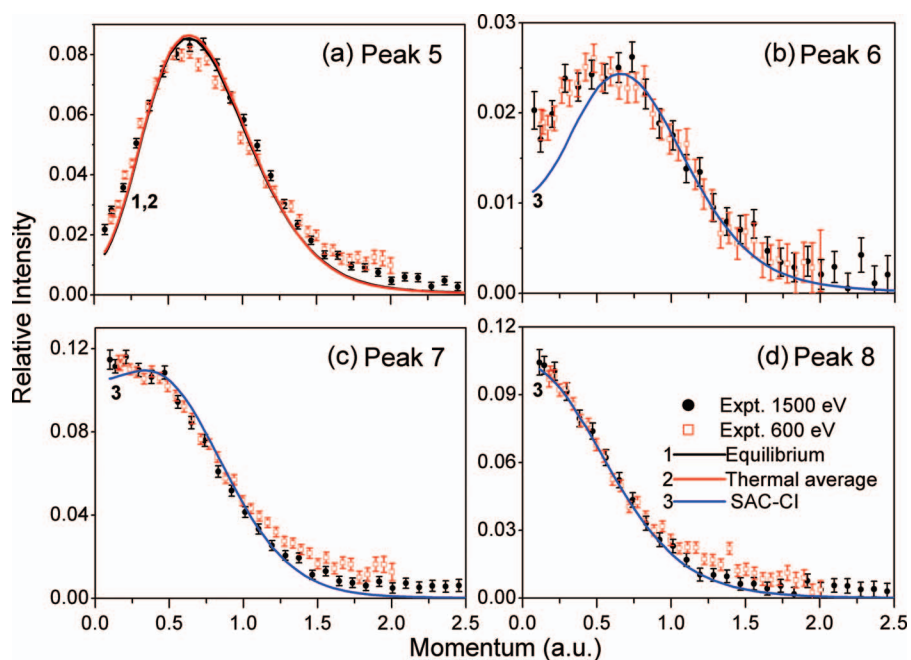


FIG. 9. Experimental and calculated momentum distributions of peak 5, 6, 7, and 8.

#### IV. SUMMARY

The binding energy spectra and electron momentum distributions of formamide were extensively investigated using the high resolution (e, 2e) spectroscopy in cooperation with the high level SAC-CI calculations. It was found that the large amplitude anharmonic vibration, the wagging motion of amino group, has noticeable effects on the momentum distributions of valence orbitals of formamide. The ionization potentials for the outer-valence orbitals and the congested satellite lines in the inner-valence region can be well reproduced by the high level SAC-CI calculation. The  $\Delta$ B3LYP method also accurately reproduced the vertical ionization potentials for formamide. In addition, it was found that the orbital energies of formamide are not sensitive to the amino-wagging vibration.

Moreover, the present work provided a solid evidence for the assignment of  $10a'$  and  $2a''$  orbitals. The highest occupied molecular orbital was ambiguously assigned to  $10a'$ . This work demonstrated the ability of electron momentum spectroscopy on determining the ordering of molecular orbitals whose energy gaps are even much smaller than the instrumental energy resolution.

#### ACKNOWLEDGMENTS

This work is supported by the National Natural Science Foundation of China (Grant Nos. 11074144, 10874097, and 11174175).

- <sup>1</sup>M. P. Bernstein, S. A. Sandford, L. J. Allamandola, S. Chang, and M. A. Scharberg, *Astrophys. J.* **454**, 327 (1995).
- <sup>2</sup>C. C. Costain and J. M. Dowling, *J. Chem. Phys.* **32**, 158 (1959).
- <sup>3</sup>R. J. Kurland and E. B. Wilson, Jr., *J. Chem. Phys.* **27**, 585 (1957).
- <sup>4</sup>W. H. Kirchhoff and D. R. Johnson, *J. Mol. Spectrosc.* **45**, 159 (1973).
- <sup>5</sup>D. R. Johnson, F. J. Lovas, and W. H. Kirchhoff, *J. Phys. Chem. Ref. Data.* **1**, 1011 (1972).
- <sup>6</sup>M. Kitano and K. Kuchitsu, *Bull. Chem. Soc. Jpn.* **47**, 67 (1974).
- <sup>7</sup>E. Hirota, R. Sugisaki, C. J. Nielsen, and G. O. Sorensen, *J. Mol. Spectrosc.* **49**, 251 (1974).
- <sup>8</sup>G. Fogarasi and P. G. Szalay, *J. Phys. Chem. A* **101**, 1400 (1997).
- <sup>9</sup>D. P. Chong, *J. Electron Spectrosc. Relat. Phenom.* **184**, 164 (2011).
- <sup>10</sup>K. Kimura, S. Katsumata, Y. Achiba, T. Yamazaki, and S. Iwata, *Handbook of HeI Photoelectron Spectra of Fundamental Organic Molecules* (Japan Scientific Societies, Tokyo, 1981).
- <sup>11</sup>L. Asbrink, A. Svensson, W. Von Niessen, and G. Bieri, *J. Electron Spectrosc. Relat. Phenom.* **24**, 293 (1981).
- <sup>12</sup>H. Siegbahn, L. Asplund, P. Kelfve, K. Hamrin, L. Karlsson, and H. Siegbahn, *J. Electron Spectrosc. Relat. Phenom.* **5**, 1059 (1981).
- <sup>13</sup>A. Lisini, M. P. Keane, S. Linell, N. Correia, A. Naves de Brito, and S. Svensson, *Chem. Phys.* **169**, 379 (1993).
- <sup>14</sup>C. E. Brion, G. Cooper, R. Feng, S. Tixier, Y. Zheng, I. E. McCarthy, Z. Shi, and S. Wolfe, "Correlations, polarization and related topics," *AIP Conf. Proc.* **604**, 38 (2002).
- <sup>15</sup>E. Weigold and I. E. McCarthy, *Electron Momentum Spectroscopy* (Kluwer Academic, New York, 1999).
- <sup>16</sup>C. E. Brion, Y. Zheng, J. Rolke, J. J. Neville, I. E. McCarthy, and J. Wang, *J. Phys. B* **31**, L223 (1998).
- <sup>17</sup>M. Takahashi, T. Saito, J. Hiraka, and Y. Udagawa, *J. Phys. B* **36**, 2539 (2003).
- <sup>18</sup>X. G. Ren, C. G. Ning, J. K. Deng, S. F. Zhang, G. L. Su, F. Huang, and G. Q. Li, *Phys. Rev. Lett.* **94**, 163201 (2005).
- <sup>19</sup>C. G. Ning, Z. H. Luo, Y. R. Huang, B. Hajgató, F. Morini, K. Liu, S. F. Zhang, J. K. Deng, and M. S. Deleuze, *J. Phys. B* **41**, 175103 (2008).
- <sup>20</sup>Z. H. Luo, C. G. Ning, K. Liu, Y. R. Huang, and J. K. Deng, *J. Phys. B* **42**, 165205 (2009).
- <sup>21</sup>M. S. Deleuze, W. N. Pang, A. Salam, and R. C. Shang, *J. Am. Chem. Soc.* **123**, 4049 (2001).
- <sup>22</sup>S. Knippenberg, Y. R. Huang, B. Hajgató, J. P. Francois, J. K. Deng, and M. S. Deleuze, *J. Chem. Phys.* **127**, 174306 (2007).
- <sup>23</sup>C. G. Ning, Y. R. Huang, S. F. Zhang, J. K. Deng, K. Liu, Z. H. Luo, and F. Wang, *J. Phys. Chem. A* **112**, 11078 (2008).
- <sup>24</sup>F. Morini, S. Knippenberg, M. S. Deleuze, and B. Hajgató, *J. Phys. Chem. A* **114**, 4400 (2010).
- <sup>25</sup>Y. Sugawara, Y. Hamada, and M. Tsuboi, *Bull. Chem. Soc. Jpn.* **56**, 1045 (1983).
- <sup>26</sup>S. T. King, *J. Phys. Chem.* **75**, 405 (1971).
- <sup>27</sup>Y. R. Miao, C. G. Ning, K. Liu, and J. K. Deng, *J. Chem. Phys.* **134**, 204304 (2011).
- <sup>28</sup>Y. R. Miao, C. G. Ning, and J. K. Deng, *Phys. Rev. A* **83**, 062706 (2011).
- <sup>29</sup>K. T. Leung and C. E. Brion, *Chem. Phys.* **82**, 87 (1983).
- <sup>30</sup>P. Duffy, D. P. Chong, M. E. Casida, and D. R. Salahub, *Phys. Rev. A* **50**, 4707 (1994).
- <sup>31</sup>I. V. Litvinyuk, Y. Zheng, and C. E. Brion, *Chem. Phys.* **253**, 41 (2000).
- <sup>32</sup>W. von Niessen, J. Schirmer, and L. S. Cederbaum, *Comput. Phys. Rep.* **1**, 57 (1984).
- <sup>33</sup>J. V. Ortiz, *J. Chem. Phys.* **89**, 6348 (1988).
- <sup>34</sup>M. A. Coplan, J. H. Moore, and J. P. Doering, *Rev. Mod. Phys.* **66**, 985 (1994).
- <sup>35</sup>C. E. Brion, *Int. J. Quantum Chem.* **29**, 1397 (1986).
- <sup>36</sup>X. G. Ren, C. G. Ning, J. K. Deng, S. F. Zhang, G. L. Su, F. Huang, and G. Q. Li, *Rev. Sci. Instrum.* **76**, 063103 (2005).
- <sup>37</sup>C. G. Ning, S. F. Zhang, J. K. Deng, K. Liu, Y. R. Huang, and Z. H. Luo, *Chin. Phys. B* **17**, 1729 (2008).
- <sup>38</sup>R. K. Singh, J. V. Ortiz, and M. K. Mishra, *Int. J. Quantum Chem.* **110**, 1901 (2010).
- <sup>39</sup>C. M. Oana and A. I. Krylov, *J. Chem. Phys.* **127**, 234106 (2007).
- <sup>40</sup>M. Yamazaki, T. Horio, N. Kishimoto, and K. Ohno, *Phys. Rev. A* **75**, 032721 (2007).
- <sup>41</sup>M. E. Casida and D. P. Chong, *Int. J. Quantum Chem.* **40**, 225 (1991).
- <sup>42</sup>R. J. F. Nicholson, I. E. McCarthy, and W. Weyrich, *J. Phys. B* **32**, 3873 (1999).
- <sup>43</sup>H. Nakatsuji, *Chem. Phys. Lett.* **59**, 362 (1978).
- <sup>44</sup>H. Nakatsuji, *Chem. Phys. Lett.* **67**, 329 (1979).
- <sup>45</sup>H. Nakatsuji and K. Hirao, *Int. J. Quantum Chem.* **20**, 1301 (1981).
- <sup>46</sup>H. Nakatsuji, *Chem. Phys.* **75**, 425 (1983).
- <sup>47</sup>H. Nakatsuji, *J. Chem. Phys.* **83**, 5743 (1985).
- <sup>48</sup>H. Nakatsuji, *J. Chem. Phys.* **94**, 6716 (1991).
- <sup>49</sup>H. Nakatsuji, *Chem. Phys. Lett.* **177**, 331 (1991).
- <sup>50</sup>H. Nakatsuji, O. Kitao, and T. Tonezawa, *J. Chem. Phys.* **83**, 723 (1985).
- <sup>51</sup>H. Nakatsuji, *J. Chem. Phys.* **113**, 2949 (2000).
- <sup>52</sup>M. Ehara, M. Ishida, and H. Nakatsuji, *J. Chem. Phys.* **114**, 8990 (2001).
- <sup>53</sup>M. Ehara, Y. Ohtsuka, H. Nakatsuji, M. Takahashi, and Y. Udagawa, *J. Chem. Phys.* **122**, 1 (2005).
- <sup>54</sup>M. Ehara, M. Ishida, and H. Nakatsuji, *J. Chem. Phys.* **117**, 3248 (2002).
- <sup>55</sup>M. Ehara and H. Nakatsuji, *Chem. Phys. Lett.* **282**, 347 (1998).
- <sup>56</sup>M. Ehara, S. Yasuda, and H. Nakatsuji, *Z. Phys. Chem.* **217**, 161 (2003).
- <sup>57</sup>J. A. Pople, J. S. Binkley, and R. Seeger, *Int. J. Quantum Chem., Symp.* **10**, 1 (1976).
- <sup>58</sup>R. J. Bartlett, *Chem. Phys. Lett.* **484**, 1 (2009).
- <sup>59</sup>J. A. Pople, R. Krishnan, H. B. Schlegel, and J. S. Binkley, *Int. J. Quantum Chem.* **14**, 545 (1978).
- <sup>60</sup>M. J. Frisch, G. W. Trucks, H. B. Schlegel *et al.*, GAUSSIAN 03, Revision E.01, Gaussian Inc., Wallingford, CT, 2004.
- <sup>61</sup>E. R. Davidson, *Chem. Phys. Lett.* **220**, 514 (1996).
- <sup>62</sup>A. D. Becke, *J. Chem. Phys.* **98**, 5648 (1993).
- <sup>63</sup>C. Lee, W. Yang, and R. G. Parr, *Phys. Rev. B* **37**, 785 (1988).
- <sup>64</sup>K. Liu, C. G. Ning, Z. H. Luo, L. L. Shi, and J. K. Deng, *Chem. Phys. Lett.* **497**, 229 (2010).
- <sup>65</sup>H. Basch, *Chem. Phys. Lett.* **37**, 447 (1976).
- <sup>66</sup>E. Lindholm, G. Bieri, L. Asbrink, and C. Frich, *Int. J. Quantum Chem.* **14**, 737 (1978).
- <sup>67</sup>W. von Niessen, *Chem. Phys.* **45**, 47 (1980).
- <sup>68</sup>M. Takahashi, R. Ogino, and Y. Udagawa, *Chem. Phys. Lett.* **288**, 821 (1998).
- <sup>69</sup>C. G. Ning, X. G. Ren, J. K. Deng, G. L. Su, S. F. Zhang, and G. Q. Li, *Phys. Rev. A* **73**, 022704 (2006).
- <sup>70</sup>ADF 2008.01, SCM, Theoretical Chemistry, Vrije Universiteit, Amsterdam, The Netherlands, 2008; G. te Velde, F. M. Bickelhaupt, E. J. Baerends, C. F. Guerra, S. J. A. van Gisbergen, J. G. Snijders, and T. Ziegler, *J. Comput. Chem.* **22**, 931 (2001).